Comparison of the Protonation of Isophosphoramide Mustard and Phosphoramide Mustard

Kevin K. Millis,† Michael E. Colvin,‡ Ellen M. Shulman-Roskes,§ Susan M. Ludeman,§ O. Michael Colvin,§ and Michael P. Gamcsik*,†

The Department of Radiology and The Oncology Center, The Johns Hopkins University School of Medicine, Baltimore, Maryland 21205, and the Center for Computational Engineering, Sandia National Laboratories, Livermore, California 94551

Received December 19, 1994®

The alkylating agent isophosphoramide mustard (IPM) spontaneously forms a relatively stable aziridine derivative which can be directly observed using NMR spectroscopy. The protonations of IPM and its aziridine were probed using ^{1}H, ^{31}P, ^{15}N, and ^{17}O NMR spectroscopy. The positions of the ^{31}P, ^{15}N, and ^{17}O resonances of IPM between pH 2 and 10 each exhibit a single monobasic titration curve with the same pK_a of 4.31 ± 0.02. On the basis of a comparison with other compounds and our earlier work with phosphoramide mustard, the NMR results for IPM indicate that protonation occurs at nitrogen and not oxygen. Over this same pH range, each of the ^{1}H, ^{31}P, and ^{15}N resonances of IPM-aziridine also show a single monobasic titration with a pK_a of 5.30 ± 0.09. The magnitude of the change in chemical shifts suggests that the protonation of the IPM-aziridine occurs at the ring nitrogen. Theoretical gas-phase calculations of PM, IPM, and IPM-aziridine suggest O-protonation to be more likely; however, aqueous phase calculations predict the N-protonated forms to be most stable. Furthermore, for PM and IPM-aziridine, which contain nonequivalent nitrogens, the theoretical calculations and experimental data both agree as to which nitrogen undergoes protonation. These results suggest that the IPM-aziridine remains unprotonated under physiological conditions and may, in part, explain the lower alkylating activity of IPM as compared to PM.

Introduction

Isophosphoramide mustard (IPM) is a metabolite of ifosfamide, one of a class of nitrogen mustard bifunctional alkylating agents used in cancer chemotherapy. Ifosfamide and cyclophosphamide are two of the most useful alkylating agents in the clinic, and although structurally related, there are significant differences in the pharmacokinetics, toxicities, and, perhaps, the efficacies of the two drugs. Both IPM and its isomer, phosphoramide mustard (PM), are produced through the activation of their parent drugs by hepatic microsomal enzymes. There are differences in the alkylating activities of IPM and PM;[1] however, both agents are believed to act via reactive aziridine/aziridinium intermediates (Scheme 1) which proceed to form cytotoxic cross-links between guanosine residues on opposite strands of DNA.[2]

This laboratory recently reported detailed studies on the protonation of PM.[3] The experimental data, supported by theoretical calculations of model compounds, suggested that protonation of PM (pK_a = 4.9) occurs at the $N^{(1)}$ position and that the pK_a of the $N^{(2)}$ nitrogen must be below pH 2. In a continuing effort to detail the chemistry of phosphoramide compounds and to determine how structure may affect activity, we present data on the protonation of IPM, a structural isomer of PM. In both isomers, any of two oxygen and two

Scheme 1

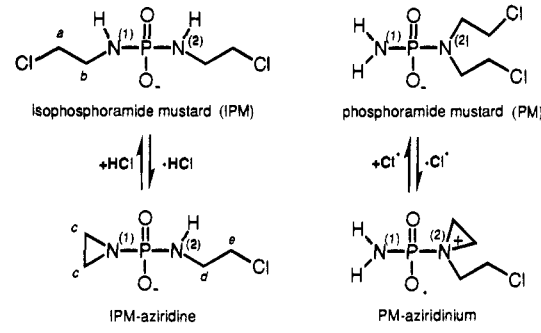

nitrogen atoms are potential protonation sites. As in the previous study of PM, our results for IPM indicate that between pH 2 and 10, a single protonation (pK_a = 4.3) occurs at a nitrogen atom rather than at an oxygen atom. For IPM, however, protonation occurs at a nitrogen which can form the reactive aziridine/aziridinium intermediate. This suggests that this nitrogen of IPM is more able to stabilize a positive charge than the $N^{(2)}$ of PM (pK_a < 2 for $N^{(2)}$ of PM). On the basis of this finding we would predict the aziridine/aziridinium of IPM to be more stable than the aziridinium of PM, and in fact, we now report the detection of a relatively stable IPM-aziridine in solution at physiological pH. Our theoretical computations show that, in acidic solution, N-protonated PM and IPM are predicted to be the most stable forms of PM and IPM. This further validates our methods used for the theoretical studies.

Results and Discussion

IPM Studies. The chemical shift of the ^{31}P NMR resonance of IPM was measured as a function of pH at 4 °C in 0.1 M NaCl. The low temperature was used to

* Address correspondence to this author at Division of NMR Research, 340 Traylor Building, 720 Rutland Avenue, Baltimore, MD 21205-2196.
† Department of Radiology, The Johns Hopkins University School of Medicine.
‡ Sandia National Laboratories.
§ The Oncology Center, The Johns Hopkins University School of Medicine.
® Abstract published in *Advance ACS Abstracts*, June 1, 1995.

0022-2623/95/1838-2166$09.00/0

Table 1. ^{31}P Chemical Shift Changes Due to Protonation

compound	Δ shift[a] (ppm)	pK_a	reference
IPM	−9.8	4.3	this work
IPM−aziridine	−13.5	5.2	this work
PM	−14.0	4.9	3
$H_2NPO_3^{2-}$	−3.2[b]	3.0	3
	−12.0[c]	8.3	3
ATP (γ-P)	−4.7	6.6	35

[a] Upfield shifts are negative, downfield shifts are positive, with decreasing pH. [b] Reflects O-protonation. [c] Reflects N-protonation.

Table 2. ^{15}N Chemical Shift Changes Due to Protonation

compound	Δ shift[a] (ppm)	pK_a	reference
IPM	7.6	4.3	this work
IPM−aziridine	3.0 (N^1)	5.3	this work
	1.7 (N^2)		
PM	12.7 (N^1)	4.9	3
	−0.4 (N^2)		
$H_2NPO_3^{2-}$	1.2[b]	2.8	3
	6.3[c]	8.2	
dimethylamine	12.9[d]	nd[e]	36
diethylamine	3.6[d]	nd	36

[a] Upfield shift are negative, downfield are positive with decreasing pH. [b] ^{15}N shift with O-protonation. [c] ^{15}N shift with N-protonation. [d] Alkylamine protonation shifts determined in methanol. [e] Not determined from ^{15}N data.

prevent breakdown of IPM in aqueous solutions. The NaCl was included in order to maintain a constant ionic strength; in addition it also acts to slow the disappearance of IPM. A single monobasic titration curve can be fit to the data resulting in the determination of a pK_a of 4.32. This value agrees with that determined previously (pK_a = 4.28 ± 0.2 at 20 °C) using similar methods.[1] The direction and magnitude of the titration shift (−9.8 ppm, i.e., upfield shift with decreasing pH) is smaller than that observed for phosphoramide mustard (−14.0 ppm) but much greater than shifts normally observed for O-protonation of phosphate groups (usually −3 to −5 ppm; Table 1). Earlier studies from our laboratory demonstrated that for phosphoramidic acid, $H_2NPO_3^{2-}$, which undergoes both N-protonation (pK_a = 8.3) and O-protonation (pK_a = 3.0), the magnitude of the pH-induced titration shift of the ^{31}P resonance is greater for N- than for O-protonation (Table 1).

Since the phosphorus nucleus is one bond away from the nitrogens and oxygens, a more direct approach is to study the nucleus at all the potential site(s) of protonation; therefore, both $^{15}N_2$-labeled IPM[4] and ^{17}O-labeled IPM[5] were prepared. The chemical shift of the ^{15}N NMR resonance of $^{15}N_2$-IPM was determined as a function of pH at 4 °C. As above, a single monobasic titration curve with a pK_a of 4.31 can be fit to the data. The pH-induced shift in the ^{15}N resonance is smaller than the shift previously observed for protonation of the $^{15}N^{(1)}$ of PM but larger than the shift observed in the nontitrating nitrogen $^{15}N^{(2)}$ of PM (Table 2). The magnitude of the change in ^{15}N chemical shift ($\Delta\delta$ = 7.6 ppm) is consistent with the data for protonation of the nitrogens of secondary amines (Table 2).

The chemical shift of the ^{17}O NMR resonance of ^{17}O-IPM was measured as a function of pH at 4 °C. Due to the broad resonances inherent in the spectrum of nonsymmetrical quadrupolar nuclei observed by NMR, the peak position could not be determined with the accuracy of the ^{31}P and ^{15}N resonances but curve fitting yields a similar pK_a value (Table 3). The monobasic titration curve with a pK_a of 4.29 and titration shift of

Table 3. ^{17}O Shifts Due to Protonation

compound	Δ shift[a] (ppm)	pK_a	reference
IPM	−2.1	4.3	this work
PM	0	nd[b]	3
sodium phosphate	−6.6	nd	37
	−12.3		
	−12.3		

[a] Upfield shifts are negative, downfield shifts are positive with decreasing pH. [b] Not determined from the ^{17}O data.

−2.1 ppm can be fit to the data. The ^{17}O NMR spectrum of ^{17}O-IPM shows a single, symmetrical broad resonance throughout the pH range studied. Previous studies of ^{17}O-PM showed changes in the peak shape but not in the position of the ^{17}O resonance with pH. The −2.1 ppm shift is smaller than would be expected if IPM underwent O-protonation. Normally O-protonation results in upfield shifts of the ^{17}O resonance of at least 6 ppm with a decrease in pH (Table 3).

The ^{31}P, ^{15}N, and ^{17}O data are all consistent with N-protonation of IPM. The average pK_a of 4.31 ± 0.02 for IPM indicates that the nitrogens of IPM can stabilize a positive charge to a greater extent than the $N^{(2)}$ nitrogen of PM (pK_a < 2).[3] These results suggest that an aziridine/aziridinium of IPM may be more stable than the aziridinium of PM. For PM, previous NMR studies could not detect an aziridinium intermediate.[1] The following sections show that the IPM−aziridine can be readily detected in solution by NMR spectroscopy.

IPM−Aziridine Studies. The preceding studies were performed at 4 °C to slow breakdown of IPM. At 37 °C, in 50 mM phosphate-buffered D_2O, pD 6.9, breakdown of the unlabeled drug follows first-order kinetics with a half-life of 75 ± 3 min (n = 3) which was determined using ^1H NMR. This value agrees with earlier ^{31}P NMR studies[1] but is longer than that found in another study ($t_{1/2}$ = 46 min).[6] In the latter study, Zheng et al.[6] measured drug breakdown by an HPLC-based method which may explain the shorter half-life observed. A previous study of phosphoramide mustard breakdown by this same laboratory showed a shorter half-life determined using this HPLC method compared to the half-life measured by the same group using ^{31}P NMR.[7]

We monitored breakdown of IPM using ^1H NMR spectroscopy. In the ^1H NMR spectrum, the loss of resonance intensity at 3.15 ppm due to the parent drug NCH_2 group is concomitant with an increase in intensity of resonances at 3.23 ppm (doublet of triplets) and 1.9 ppm (doublet) (Figure 1). The relative integrated intensity of these new resonances is 2:4, respectively. The position, multiplicity, and intensity of these resonances are consistent with their assignment to the protons of IPM−aziridine. The resonance at 3.23 ppm is similar in position and multiplicity to the resonance (NCH_2) of the parent drug and can be assigned to the α-methylene protons of the chloroethylamine moiety of the IPM−aziridine (protons labeled *d* in Scheme 1). The resonance for the β-protons of the chloroethylene moiety of the IPM−aziridine (protons labeled *e* in Scheme 1) has essentially the same chemical shift (3.6 ppm) as the β-protons of the chloroethylene moiety of IPM (protons labeled *a* in Scheme 1). The presence of these resonances beneath the protons of the starting material can be detected by subtraction of the spectra (data not shown). The overall resonance intensity at 3.6 ppm does

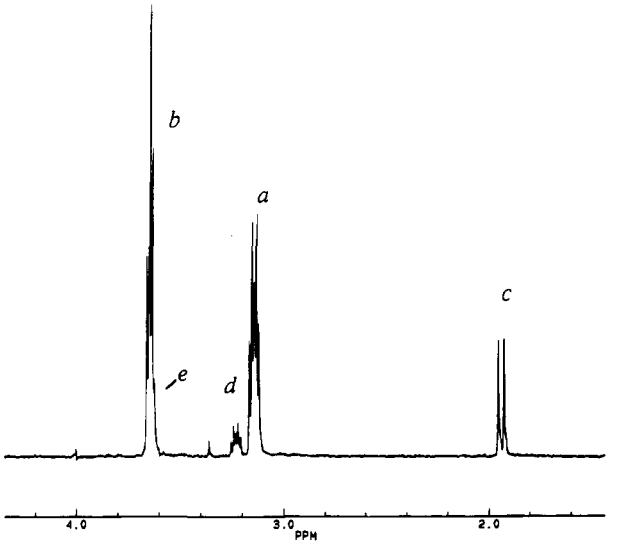

Figure 1. The 500.13 MHz ^1H NMR spectrum of IPM and IPM–aziridine in 50 mM phosphate, D_2O, pD 6.9. The methylene proton assignments are shown and correspond to the labels (a–e) in Scheme 1.

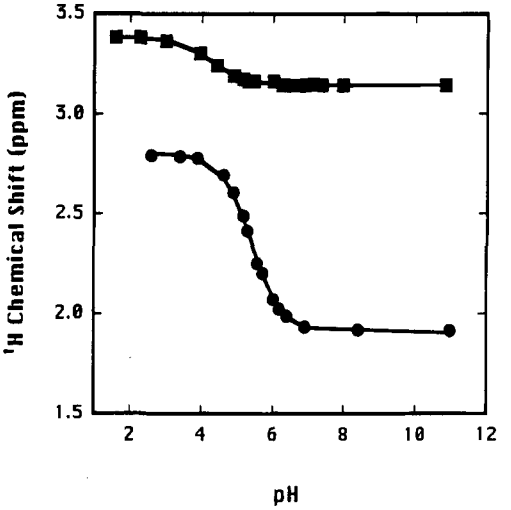

Figure 2. The ^1H NMR chemical shifts of IPM (squares) and IPM–aziridine (circles) as a function of pH at 4 °C. For IPM, $pK_a = 4.25 \pm 0.05$; as determined from the ring protons "c" of IPM–aziridine, $pK_a = 5.39 \pm 0.02$.

not change with aziridine formation. The upfield doublet at 1.9 ppm is due to the equivalent protons of a rapidly inverting aziridine ring (protons labeled c in Scheme 1) split by the heteronuclear scalar coupling to the phosphorus nucleus ($^3J(^1H-^{31}P) = 13.9$ Hz). Without the scalar coupling to the phosphorus, the ring protons would appear as a singlet. We confirmed this by preparing aziridine (ethylenimine) and recording the ^1H NMR spectrum under identical conditions and finding that the ring protons appear as a singlet at 2.6 ppm. Hindered inversion of the ring nitrogen in IPM–aziridine would lead to a more complex ^1H NMR spectrum due to the nonequivalence of the ring protons on a tetrahedrally substituted nitrogen atom. For example, the aziridinium ring protons of mechlorethamine exhibit a more complex AA'BB' coupling pattern in the ^1H NMR spectrum.[8,9] The appearance of the ring proton resonances as a sharp doublet suggests that the ring nitrogen for IPM–aziridine is not protonated at physiological pH.

Once sufficient aziridine had formed, typically ~25% of the reaction in 30 min, the sample was cooled to slow further breakdown. It should be noted, however, that even at 4 °C, IPM–aziridine does undergo a slow decomposition as evidenced by the appearance of other small resonances in the NMR spectra. The shift in resonance position of the ring protons was measured as a function of pH and a curve fit of the data results in the determination of a $pK_a = 5.4$ for the IPM–aziridine (Figure 2). The ^1H NMR resonances of the ring protons shift downfield 0.9 ppm with decreasing pH. This titration shift is larger than the shift observed for the NCH_2 protons of IPM (titration shift of 0.25 ppm). The ring protons remain as a doublet throughout the pH range shown in Figure 2; however, the resonances broaden and the heteronuclear scalar coupling changes at low pH ($^3J(^1H-^{31}P) = 5.8$ Hz at pH 1.6) until the resonance broadens beyond detectability (pH 0.7). Although the AA'BB' pattern typical of an aziridinium was not present at pH 1.6, the broadening of the doublet may indicate that the exchange rate of the proton(s) on $N^{(1)}$ of IPM–aziridine changes. Further broadening at pH 0.7 suggests that, below this pH, proton exchange rates may be sufficiently slow to produce the expected coupling pattern of the aziridinium ion.

In the ^{31}P NMR spectrum, incubation of IPM ($\delta = 11.4$ ppm) at 37 °C results in the appearance of a resonance at 15.4 ppm (pH 7.0). In the nondecoupled ^{31}P NMR spectrum, this resonance appears as a complex multiplet. Selective irradiation at the aziridine ring proton resonance frequency during acquisition of the free induction decay changes this multiplicity to a triplet proving that the ^{31}P NMR resonance at 15.4 ppm is due to the IPM–aziridine. Titration of the sample at low temperature results in the data shown in Table 1. The pK_a of 5.22 obtained from the ^{31}P NMR data is consistent with that obtained for the IPM–aziridine by ^1H NMR spectroscopy. The magnitude of the ^{31}P NMR shift (−13.5 ppm) is larger than that observed for the parent drug. Both shifts, however, suggest that N-protonation occurs in each case (Table 1).

Formation of IPM–aziridine from $^{15}N_2$-IPM was followed by ^1H, ^{31}P, and ^{15}N NMR. Initially, the proton-decoupled ^{31}P NMR spectrum of $^{15}N_2$-IPM is a well-resolved triplet (11.4 ppm) due to heteronuclear coupling between the phosphorus and the two equivalent ^{15}N-labeled nitrogens ($^1J(^{31}P-^{15}N) = 29.0$ Hz (pH 6.9); Figure 3a). With aziridine formation, these nitrogens are now nonequivalent, resulting in the appearance of a doublet of doublets in the ^{31}P NMR spectrum centered at 15.4 ppm (see inset Figure 3a). The phosphorus nucleus of $^{15}N_2$-IPM–aziridine shows heteronuclear scalar coupling to two nonequivalent ^{15}N-labeled nitrogens ($^1J(^{31}P-^{15}N) = 29.0$, 12.1 Hz). The coupling constants can be assigned to specific phosphorus–nitrogen interactions after analysis of the ^{15}N NMR spectra.

The ^{15}N NMR spectra of $^{15}N_2$-IPM and its aziridine are shown in Figure 3b,c. The spectra shown were acquired from a solution at pH 9.1 in order to easily distinguish small coupling constants. As the pH of the solution approaches the pK_as of both IPM and IPM–aziridine, the spectra broaden, obscuring some of the scalar couplings. In the proton-decoupled ^{15}N NMR spectrum (pH 9.1), the resonance of $^{15}N_2$-IPM appears as a doublet due to the heteronuclear scalar coupling to the phosphorus. As aziridine is formed, two reso-

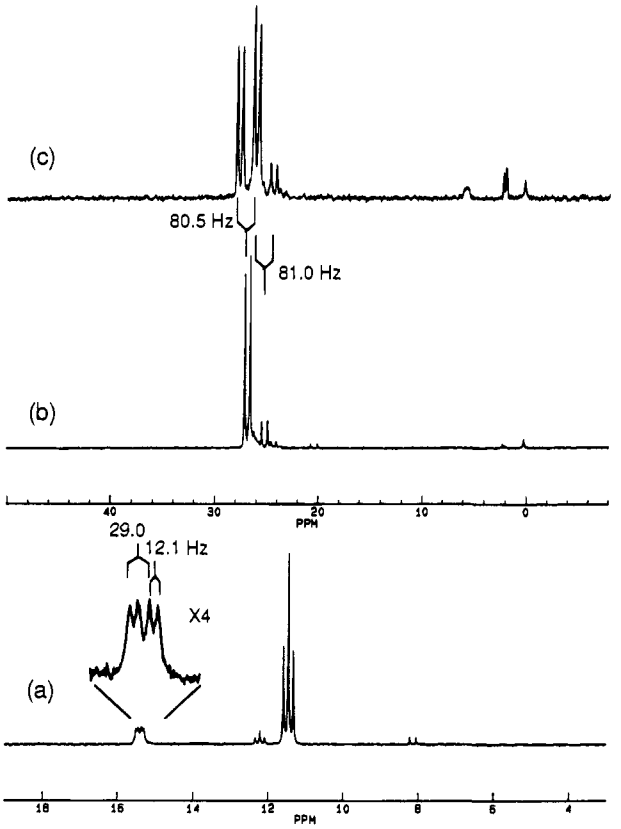

Figure 3. (a) The 202.5 MHz ^{31}P NMR spectrum of $^{15}N_2$-IPM and $^{15}N_2$-IPM−aziridine in H_2O (5% D_2O), pH 6.9, 4 °C. The inset to this spectrum shows an approximately 4-fold expansion of the ^{15}N-IPM−aziridine resonances. The 50.7 MHz ^{15}N NMR spectrum of ^{15}N-IPM and ^{15}N-IPM−aziridine with (b) and without (c) broadband proton decoupling in H_2O (5% D_2O) at pH 9.1, 4 °C.

nances appear in addition to that of $^{15}N_2$-IPM (Figure 3b). One resonance with the larger coupling constant (29.0 Hz) appears at 25.2 ppm, just upfield of the ^{15}N resonance of IPM at 26.9 ppm. Located further upfield of these resonances is another resonance at 2.2 ppm with the smaller (12.1 Hz at pH 6.5; 13.7 Hz at pH 9.1) coupling constant (at pH 9.1 and using the parameters to acquire Figure 3b, the resonance at 2.2 ppm is of very low intensity which may be due to a long longitudinal relaxation time and/or unfavorable Overhauser effects). In the proton-coupled ^{15}N NMR spectrum of this sample at pH 9.1 (Figure 3c), the $^{15}N_2$-IPM resonance and the resonance at 25.2 ppm show large scalar couplings to protons ($^1J(^1H-^{15}N)$ = 80.5, 81.0 Hz, respectively); the upfield ^{15}N resonance at 2.2 ppm shows a much smaller proton coupling (<2 Hz) which is not directly measurable in the ^{15}N NMR spectrum but results in a broadening of the resonances. Both the 25.2 and 2.2 ppm resonances show a 2.9 Hz coupling from the two-bond $^{15}N-^{15}N$ scalar interaction due to the nonequivalence of the two nitrogens in IPM−aziridine.

In order to assign these ^{15}N resonances, selective ^{15}N decoupling was used during observation of the ^1H NMR spectrum. Selective decoupling at the ^{15}N resonance at 2.2 ppm during acquisition of the ^1H NMR spectrum resulted in disappearance of the heteronuclear $^1H-^{15}N$ scalar coupling causing an increase in the intensity of the ring proton resonances at 1.9 ppm (data not shown). The ^{15}N resonances at 2.2 and 25.2 ppm can, therefore, be assigned to the ring and chloroethylamine nitrogens, respectively. The chemical shifts of these resonances as a function of pH were obtained at low temperature. Curve fitting of the data yields a pK_a of 5.29 with a titration shift of 3.0 ppm for the ring nitrogen ($N^{(1)}$ and a pK_a of 5.29 and titration shift of 1.7 ppm for the $N^{(2)}$ (Table 2). The greater magnitude of the pH-induced shift of the ring nitrogen ^{15}N resonance suggests that this is the nitrogen being protonated. This protonation at $N^{(1)}$ results in a smaller shift in the resonance of the nontitrating $N^{(2)}$ nitrogen of IPM−aziridine.

The ^{31}P data for IPM−aziridine (Table 1) suggests N-protonation occurs. The ^{15}N data for $^{15}N_2$-IPM−aziridine (Table 2) suggests that the ring nitrogen is most likely the site of this protonation. The magnitude of the pH-induced chemical shifts in the ^1H NMR spectrum of the ring protons (Figure 2) also implicates $N^{(1)}$ as the protonation site. The failure to see a change in the multiplicity of the ^1H NMR spectrum of ring protons at low pH implies that proton exchange and ring inversion are still rapid for the IPM−aziridinium. The observed broadening of these resonances with decreasing pH may indicate changes in the proton-exchange and ring-inversion rates. The observation of a large scalar coupling (at pH 9.1) between protons and ^{15}N in the ^{15}N NMR resonances of $^{15}N_2$-IPM and the $^{15}N^{(2)}$ of $^{15}N_2$-IPM−aziridine indicates that these nitrogens contain one proton.

The fitted titration curves for IPM and IPM−aziridine showing the change in ^{31}P, ^{15}N, and ^{17}O chemical shifts as a function of pH are contained in the supplementary material.

Theoretical Studies. Previous studies suggested that the differences in the alkylation rate between PM, IPM, and other analogs are due to differences in electron density at the nitrogens.[1,10] We have, therefore, performed *ab initio* quantum chemical calculations on protonated forms of PM, IPM, and IPM−aziridine and compared these results with our experimental data. In a previous study, theoretical calculations predicted that O-protonated forms of some small phosphoramide model compounds were more stable than their N-protonated counterparts in the gas phase. However, using a polarizable continuum model to mimic the effect of aqueous solvation, the N-protonated forms, in many cases, were predicted to be more stable.[3]

The different protonated forms of PM, IPM, and IPM−aziridine are shown in Figure 4. The structures were optimized at the self-consistent field (SCF) level of theory using the 6-31G* basis set. Selected bond lengths and of the optimized structures are listed in Table 4. (The complete internal coordinate Z matrices for these structures are provided in the supplementary material.) Different conformations of the floppy chloroethyl "arms" of the nitrogen mustard groups lead to nearly degenerate ground state structures for IPM and PM. This folding creates slightly asymmetric chemical environments for the stereochemically identical moieties such as the oxygens in IPM. As a result, these groups exhibit slightly different bond lengths and charge densities.

The data in Table 4 reveal some unique features of the complex bonding structure of the phosphoramide center in the gas phase. The bonding of phosphorus to nitrogen and other first-row elements has long been described in terms of p_π to d orbital backbonding;

Table 4. Selected Bond Lengths (Å) and Angles (deg) of the Structures in Figure 4

bond length or angle	structure														
	1a	**1b**	**1c**	**1d**	**2a**	**2b**	**2c**	**2d**	**2e**	**3a**	**3b**	**3c**	**3d**	3e	**3f**
P–N²	1.650	1.826	1.729	1.928	1.658	1.884	1.674	1.739	1.795	1.654	1.604	1.816	1.721	1.653	1.929
P–N¹	1.668	1.612	1.712	1.660	1.644	1.656	1.905	1.702	1.611	1.656	1.859	1.620	1.718	1.955	1.662
P–O2	1.599	1.569	1.479	1.457	1.602	1.458	1.459	1.477	1.573	1.601	1.565	1.569	1.480	1.454	1.458
P–O3	1.453	1.438	1.480	1.456	1.460	1.461	1.458	1.480	1.439	1.459	1.437	1.439	1.480	1.454	1.458
C–Cl	1.794	1.775	1.818	1.792	1.795	1.797	1.789	1.827	1.778	1.795	1.778	1.775	1.825	1.795	1.793
C–Cl	1.790	1.773	1.822	1.789						1.793	1.777	1.776	1.825	1.795	1.791

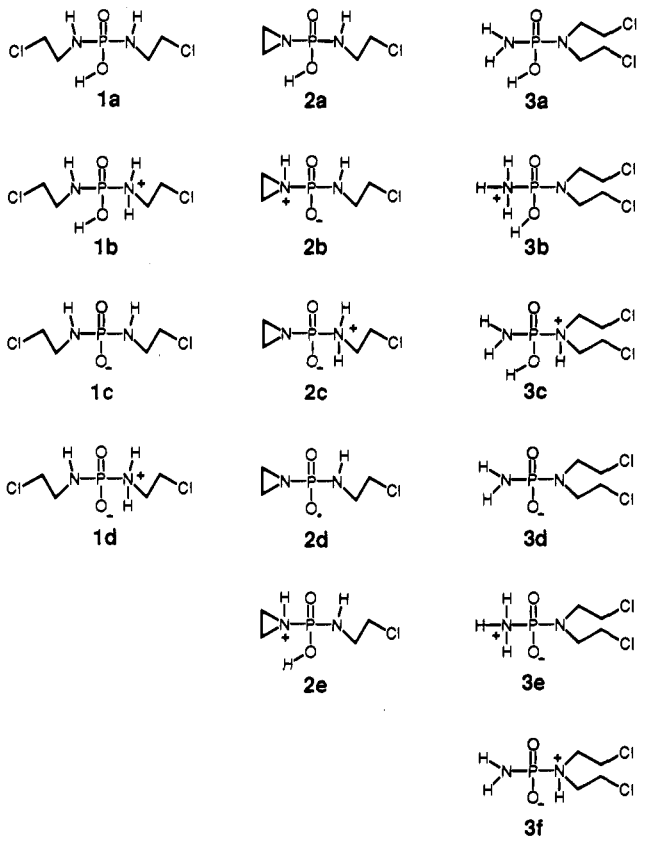

Figure 4. Protonated forms of IPM, IPM–aziridine, and PM.

however, more recent studies by Reed and Schleyer[11] have shown that this interaction is more properly described in terms of "negative hyperconjugation". For a phosphoramide, X_3PN, the P–N negative hyperconjugation involves overlap between nitrogen p_π orbitals and the P–X σ^*-antibonding orbitals. In each case, protonating a nitrogen inhibits the nitrogen lone pair from participating in the negative hyperconjugation yielding a much longer P–N "single" bond length of 1.82–1.96 Å (structures **1b**, **1d**, **3b**, **3c**, **3e**, and **3f**, Figure 4) as compared to shorter bond lengths of 1.65–1.73 Å (**3a**, **3d**, **1a**, **1c**) when the nitrogen lone pairs are available for negative hyperconjugation. Similarly, deprotonating the hydroxyl group allows oxygen p_π to phosphorus negative hyperconjugation yielding nearly equivalent P–O bond lengths of ~1.48 Å.

Unfortunately, no experimental structural data is available for IPM and PM; however, X-ray crystal structures of cyclophosphamide[12,13] and 4-hydroperoxyifosfamide[14] have been reported. In these compounds, P=O bond lengths are reported to be between 1.47 and 1.53 Å and P–O bonds range from 1.57 to 1.58 Å. The single P–N bond length ranges from 1.58 to 1.66 Å. These data compare favorably with our theoretical calculations for the mustards.

The interaction with a polar solvent can be expected to modify these structures. Using the continuum dielectric solvent model it is possible to calculate the solvent-induced force on the atoms and estimate the resulting change in equilibrium bond lengths. For zwitterionic PM (**3e**), the strongest of these solvent induced forces act to increase the bond length of the phosphorus–oxygen bonds; essentially acting to pull the negatively charged oxygens into the solvent. The predicted magnitude of these forces are approximately 0.06 Hartree/Bohr, large enough to cause significant elongation in the bond length. The effects of solvation on these structures will be investigated in detail in a later paper.

Using the optimized geometries, the gas-phase second-order (MP2) Møller–Plesset perturbation theory energies as well as the (Hartree–Fock) HF vibrational zero point energies (ZPE) were calculated (Table 5). The expected error bars for gas-phase thermodynamic properties are not characterized as well as those for the structural properties; however, investigations of similar classes of compounds suggest that the relative MP2 energies should be accurate to within a few kcal/mol.[15]

The components of the aqueous solvation energy and the total aqueous free energy also are given in Table 5. G_{elec} lists the electrostatic free energy of solvation. The cavitation term, G_{cav}, is the energy required to form a "solute-sized" cavity in the water and should be similar for the structures in Figure 4 which have nearly identical molecular volumes and surface areas. The value of G_{solv} is calculated as the sum of G_{cav} and G_{elec}.

Table 5 lists the total calculated free energies for neutral, anionic, cationic, and zwitterionic forms of IPM, IPM–aziridine, and PM. There are large systematic errors associated with comparing *ab initio* energies for systems with different net charges due to the fact that a finite basis set is used to describe the electronic wave function. Therefore, we have chosen to limit our quantitative comparisons to compounds with the same net charge. A comparison of the gas-phase energies of all species with a net charge of zero shows that, in each case, the O-protonated forms are more stable than the N-protonated forms. As in our previous study with phosphoramide model compounds, the prediction of O-protonation in the gas phase is not unexpected[3] and parallels theoretical and experimental data for the protonation of glycine.[16,17]

A comparison of aqueous phase energies for all species with a net zero charge shows a change in relative energies from that found in the gas phase. These results show that in solution, the N-protonated form of IPM (**1d**) is more stable than the O-protonated form (**1a**). These predictions are consistent with our experimental observations. Similarly, our previous experimental work suggested that protonation of PM occurs at the $N^{(1)}$ nitrogen,[3] and now our theoretical results

Table 5. Gas Phase and Aqueous Phase Energies of N- and O-Protonated Structures in Figure 4

structure	MP2/6-31G** (Hartrees)	ZPE (Hartrees)	S (cal/deg mol)	total G (Hartrees)	G_{elec} (kcal/mol)	G_{cav} (kcal/mol)	G_{sol} (kcal/mol)	total G (solv) (Hartrees)
1a	−1677.927 074	0.183 580	122.926	−1677.801 900	−42.4	22.5	−19.9	−1677.833 647
1b	−1678.277 182	0.198 695	122.647	−1678.136 760	−101.9	22.8	−79.1	−1678.262 851
1c	−1677.388 851	0.171 012	120.530	−1677.275 106	−88.3	22.3	−66.0	−1677.380 266
1d	−1677.919 723	0.186 993	120.775	−1677.790 113	−50.9	22.3	−28.6	−1677.835 736
2a	−1217.679 944	0.168 519	108.199	−1217.562 835	−26.4	19.7	−6.6	−1217.573 403
2b	−1217.673 803	0.171 225	106.106	−1217.552 992	−46.4	19.6	−26.8	−1217.595 774
2c	−1217.663 709	0.171 766	107.504	−1217.543 022	−43.3	19.5	−23.8	−1217.580 878
2d	−1217.132 764	0.155 783	104.651	−1217.026 704	−90.7	19.2	−71.5	−1217.140 573
2e	−1218.038 471	0.182 970	109.832	−1217.907 685	−90.8	20.1	−70.7	−1218.020 278
3a	−1677.936 426	0.183 482	114.001	−1677.807 109	−31.2	21.6	−9.6	−1677.822 365
3b	−1678.275 163	0.197 830	117.825	1678.133 316	−104.6	22.1	−82.5	−1678.264 821
3c	−1678.276 987	0.198 127	112.940	−1678.132 521	−91.1	21.3	−69.7	−1678.243 672
3d	−1677.397 426	0.170 370	113.420	−1677.280 945	−77.3	21.5	−55.8	−1677.369 857
3e	−1677.922 657	0.185 753	115.924	−1677.791 983	−49.5	21.7	−27.7	−1677.836 171
3f	−1677.922 806	0.186 856	110.604	−1677.788 501	−40.7	21.0	−19.7	−1677.819 867

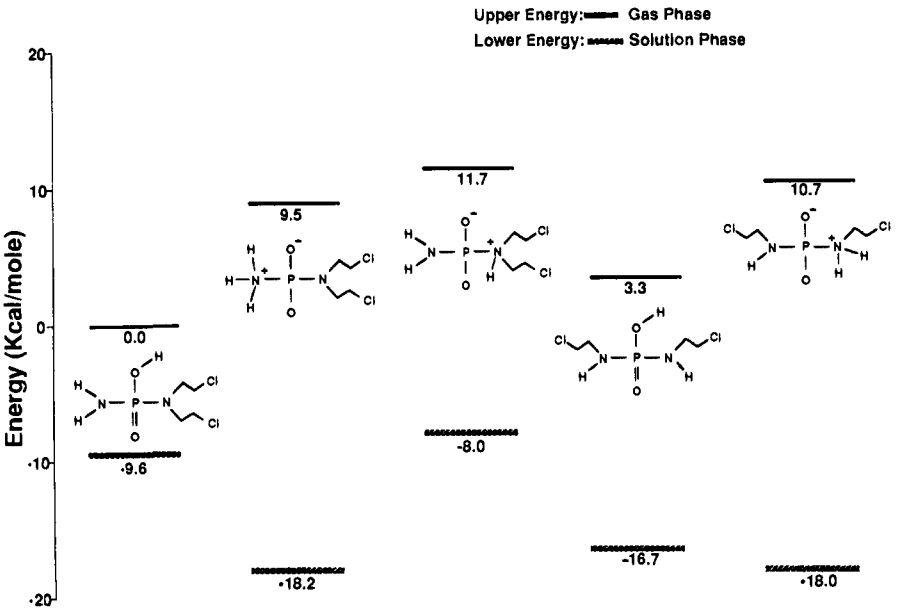

Figure 5. Relative energies of neutral IPM and PM species.

show that this is predicted to be the site of protonation in aqueous solution.

For the IPM−aziridine, both of the N-protonated forms (**2b**,**c**) are predicted to be more stable than the O-protonated neutral IPM−aziridine (**2a**) with the ring $N^{(1)}$-protonated form (**2b**) found to be most stable. The NMR evidence suggests that the ring nitrogen in IPM is protonated with a pK_a of 5.3 and verifies these predictions.

A summary of the gas and aqueous phase data is shown in Figures 5 and 6. In Figure 5, the total free energy (in kcal/mol) of all IPM and PM species with a net charge of zero are shown schematically relative to the gas-phase energy of the neutral PM structure (**3a**). The IPM−aziridine energies are computed relative to the gas-phase energy of the neutral IPM−aziridine (**2a**). It is interesting to note that there is a relatively small energy difference between the two IPM structures (**1a** and **1d**) in aqueous solution (−16.7 vs −18.0 kcal/mol) corresponding to a difference of only one pK_a unit. This may suggest that a significant population of IPM exists in both forms. We previously noted that the magnitude of the pH-induced ^{15}N and ^{31}P titration shifts for IPM are smaller and the ^{17}O shift is larger than for PM. This is consistent with a fraction of the population of IPM existing in the O-protonated form since, for PM, the corresponding energy differences between the N- and O-protonated forms (**3e** and **3a**, respectively) are much larger, thereby decreasing the likelihood of the presence of O-protonated PM.

Much of the published discussions of phosphoramide mustard reactivities have been in terms of the atomic charges on the nitrogens and oxygens.[1,3,10,18,19] In terms of true physical observables, the concept of atomic charge is not well defined because the electrons are a diffuse charge distribution that can be arbitrarily assigned to any atomic center. Nevertheless, because of the general utility of the concept of atomic charges, a number of methods have been developed for calculating them from quantum chemical wave functions.[20] Mulliken population analysis (MPA) has a long history and is still the most commonly used method to calculate atomic charges, but the MPA charges are extremely basis-set dependent, particularly for atoms with extended electron clouds, such as phosphorus, and frequently yield unintuitive results. Natural population analysis (NPA)[21] remedies the basis set dependence and other deficiencies of MPA and has been important in explaining the properties of hypervalent atomic centers, including phosphate.[11]

Both MPA and NPA involving partitioning the charge into orbitals. A very different approach is to determine

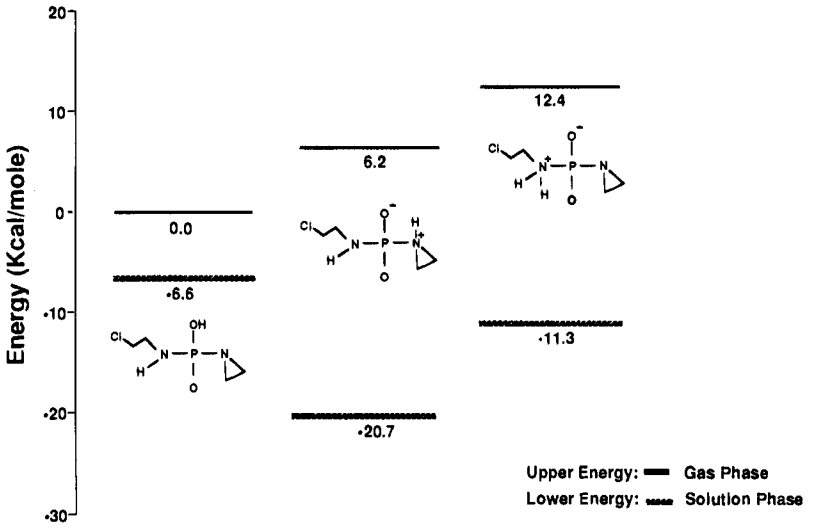

Figure 6. Relative energies of neutral IPM−aziridine species.

atomic charges that reproduce the long-range electrostatic "profile" of the molecule. Our fitting procedure predicts the atomic charges that most accurately reproduce the net dipole moment of the molecule and the electrostatic field at the solvent accessible surface. In comparison to the orbital based methods, such fitted charges better describe the long-distance electronic properties of the molecule[22] and hence are useful for molecular dynamics calculations.[23]

Since these methods have different strengths, we have calculated the gas-phase atomic charges using all three methods (as well as the aqueous phase fitted charges), although the bulk of the discussion will focus on the more reliable NPA charges. The charges for the phosphorus and all phosphorus-bound heteroatoms are given in Table 6. A complete tabulation of the atomic charges is provided in the supplementary material.

The first question that must be addressed is how the calculated atomic charges vary between the different chemical species and between different protonation states of the molecules. The charges given in Table 6 show that the MPA atomic charges generally follow the trends seen for the NPA charges. However, in some cases, the MPA charges contradict the NPA results, yielding unintuitive results. For instance, the tertiary nitrogen in **2a** gains negative charge when protonated in **2e**. The MPA charges also exhibit an overall 2−3 times larger variability for the individual atom types than the NPA charges. The most striking fact about the NPA charges is that there is very little variation in the charges of particular types of heteroatoms. Over the entire set of molecules, most of the heteroatoms exhibit charge shifts of just a few hundredths of an electron. For example, the unprotonated secondary nitrogens have an atomic charge ranging from −1.12 and −1.17, regardless of the net charge and the protonation state of the molecule or whether the compound contains an aziridinium. Similarly, the unprotonated primary and tertiary nitrogens have charges in the range of −1.31 to −1.37 and −0.90 to −0.98, respectively. Note that the tertiary nitrogens include those with bis(chloroethyl) moieties and those in aziridine rings, which are found to have nearly identical atomic charges.

Although the fit atomic charges (Fit(gas), Fit(aq)) should yield the most accurate long-range electrostatics, their dependence on the molecular geometry limit their usefulness in explaining chemical properties. This strong configurational dependence of the fit charges is especially evident in the phosphorus charge, which varies by more than 0.3 electron between the different neutral species, as compared to a variation of only 0.01 electron for the NPA method (Table 6). Nevertheless, trends between the gas and aqueous phase fit charges are consistent enough to provide some insight into how solvation affects the charge distribution. As one would expect, aqueous solvation increases the polarization of the compounds. Interestingly, the bulk of this polarization occurs along the P−O bonds, with the P typically losing 0.1−0.2 electron to the oxygens (Table 6). In contrast, the P−N bonds exhibit relatively little polarization upon solvation. With the exception of the anionic species, the C−Cl bonds are also strongly polarized by solvation, with typically 0.1 electron moving from the C to the Cl.

In comparing the NPA charges of the different types of heteroatoms, the results bear out most of the intuitive notions of charge distributions. For example the ordering of the atomic charge of the amines, NH_2 > $NH(CH_2CH_2Cl)$ > $N(CH_2CH_2Cl)_2$ reflects both the chemical notion that the chloroethyl groups act as electron-withdrawing groups and the measured pK_a values for chloroethylamines.[24] Similarly, protonating the nitrogens lowers their charges by ~0.2 electron.

It is intriguing to relate these nitrogen charges to the rate of aziridinium formation, particularly since Cohen et al.[24] found that the cyclization rate was proportional to K_a for some chloroethylamines, and Boal et al.[1] suggested that *ab initio* calculations of the nitrogen charges might explain the unusually slow alkylation rate of IPM relative to PM. Our computed charges do not suggest that the IPM nitrogen would be less nucleophilic than the PM tertiary nitrogen. Instead the secondary nitrogens in IPM have ~0.2 electron greater charge than the PM tertiary nitrogen and hence would be expected to better nucleophiles (Table 6). Interestingly, the nitrogen charges suggest that, if unprotonated, the PM primary amine would be significantly more nucleophilic than the tertiary amine and provide a competitive cyclization reaction to form a five-membered ring.[25]

Table 6. HF/6-31G** Atomic Charges for Selected Atoms Calculated at the HF/6-31G* Optimized Geometries Using Natural Population Analysis (NPA), Mulliken Population Analysis (MPA), and Fits to the Charge at the Solvent-Accessible Surface in the Gas Phase (Fit(gas)) and a Continuum Dielectric Solvent Model (Fit(aq))[a]

species	atom type	NPA	MPA	Fit(gas)	Fit(aq)	species	atom type	NPA	MPA	Fit(gas)	Fit(aq)
1a	P	2.72	1.57	1.67	1.75	**3a**	P	2.71	1.57	1.33	1.44
	O[b]	−1.08	−0.69	−0.76	−0.85		O[b]	−1.10	−0.72	−0.65	−0.72
	=O	−1.20	−0.71	−0.79	−0.94		=O	−1.21	−0.73	−0.78	−0.89
	N	−1.15	−0.85	−0.91	−0.90		N (3°)	−0.97	−0.82	−0.37	−0.38
	N	−1.14	−0.83	−1.00	−0.98		N (1°)	−1.31	−0.86	−0.95	−1.01
	Cβ	0.09	0.07	0.25	0.32		Cβ	0.09	0.06	0.22	0.30
	Cl	−0.11	−0.11	−0.28	−0.37		Cl	−0.11	−0.11	−0.25	−0.33
	Cβ	0.08	0.05	0.29	0.39		Cβ	0.08	0.06	0.24	0.32
	Cl	−0.10	−0.09	−0.28	−0.37		Cl	−0.10	−0.10	−0.25	−0.33
1b	P	2.72	1.61	1.47	1.58	**3b**	P	2.73	1.64	1.25	1.40
	O[b]	−1.10	−0.69	−0.67	−0.70		O[b]	−1.10	−0.69	−0.62	−0.67
	=O	−1.15	−0.64	−0.69	−0.82		=O	−1.14	−0.64	−0.66	−0.79
	N	−1.17	−0.83	−0.92	−0.95		N (3°)	−0.99	−0.81	−0.36	−0.39
	N^+	−0.97	−0.79	−0.60	−0.55		N^+ (1°)	−1.14	−0.82	−0.62	−0.68
	Cβ	0.05	0.04	0.16	0.28		Cβ	0.08	0.08	0.23	0.29
	Cl	−0.04	−0.02	−0.17	−0.33		Cl	−0.05	−0.03	−0.17	−0.31
	Cβ	0.08	0.09	0.24	0.31		Cβ	0.07	0.07	0.26	0.32
	Cl	−0.02	0.00	−0.15	−0.29		Cl	−0.05	−0.03	−0.18	−0.31
1c	P	2.70	1.49	1.59	1.67	**3c**	P	2.71	1.65	1.31	1.42
	O	−1.28	−0.83	−0.88	−0.98		O[b]	−1.10	−0.72	−0.61	−0.65
	O	−1.28	−0.82	−0.94	−1.05		=O	−1.15	−0.64	−0.67	−0.80
	N	−1.12	−0.83	−0.93	−0.90		N^+ (3°)	−0.83	−0.80	−0.18	−0.17
	N	−1.13	−0.83	−0.95	−0.98		N (1°)	−1.34	−0.87	−1.01	−1.03
	Cβ	0.10	0.05	0.24	0.33		Cβ	0.07	0.06	0.23	0.30
	Cl	−0.17	−0.19	−0.36	−0.39		Cl	−0.02	0.01	−0.12	−0.26
	Cβ	0.11	0.09	0.23	0.29		Cβ	0.08	0.08	0.33	0.40
	Cl	−0.18	−0.20	−0.38	−0.40		Cl	−0.02	0.00	−0.17	−0.29
1d	P	2.70	1.56	1.57	1.63	**3d**	P	2.72	1.55	1.40	1.46
	O	−1.22	−0.77	−0.80	−0.91		O	−1.29	−0.85	−0.86	−0.95
	O	−1.22	−0.75	−0.83	−0.94		O	−1.29	−0.85	−0.86	−0.95
	N^+	−0.95	−0.78	−0.54	−0.44		N (3°)	−0.96	−0.82	−0.63	−0.56
	N	−1.16	−0.85	−1.00	−0.99		N (1°)	−1.37	−0.92	−1.08	−1.13
	Cβ	0.07	0.04	0.21	0.31		Cβ	0.16	0.13	0.28	0.33
	Cl	−0.10	−0.10	−0.27	−0.36		Cl	−0.21	−0.23	−0.37	−0.39
	Cβ	0.11	0.10	0.31	0.34		Cβ	0.16	0.12	0.27	0.31
	Cl	−0.09	−0.08	−0.25	−0.32		Cl	−0.21	−0.23	−0.36	−0.38
2a	P	2.72	1.55	1.41	1.56	**3e**	P	2.71	1.59	1.32	1.40
	O[b]	−1.10	−0.71	−0.71	−0.77		O	−1.21	−0.75	−0.77	−0.87
	=O	−1.22	−0.74	−0.80	−0.91		O	−1.21	−0.75	−0.77	−0.87
	N (3°)	−0.94	−0.68	−0.38	−0.49		N (3°)	−0.98	−0.83	−0.42	−0.39
	N (2°)	−1.14	−0.81	−0.83	−0.88		N^+ (1°)	−1.13	−0.83	−0.52	−0.57
2b	P	2.70	1.53	1.46	1.54		Cβ	0.10	0.08	0.28	0.32
	O	−1.22	−0.75	−0.79	−0.89		Cl	−0.11	−0.11	−0.27	−0.34
	O	−1.21	−0.74	−0.83	−0.93		Cβ	0.10	0.08	0.26	0.30
	N (3°)	−0.97	−0.74	−0.45	−0.48		Cl	−0.11	−0.11	−0.26	−0.34
	N^+ (2°)	−0.95	−0.77	−0.63	−0.58	**3f**	P	2.69	1.59	1.43	1.46
2c	P	2.71	1.58	1.40	1.47		O	−1.22	−0.76	−0.81	−0.90
	O	−1.22	−0.75	−0.79	−0.90		O	−1.23	−0.78	−0.82	−0.91
	O	−1.23	−0.78	−0.80	−0.91		N^+ (3°)	−0.79	−0.78	−0.06	0.02
	N^+ (3°)	−0.80	−0.69	−0.31	−0.35		N (1°)	−1.34	−0.90	−1.04	−1.02
	N (2°)	−1.15	−0.84	−0.84	−0.80		Cβ	0.12	0.10	0.29	0.31
2d	P	2.71	1.53	1.52	1.59		Cl	−0.09	−0.09	−0.24	−0.29
	O	−1.27	−0.83	−0.88	−0.98		Cβ	0.11	0.10	0.31	0.35
	O	−1.28	−0.84	−0.91	−1.00		Cl	−0.09	−0.08	−0.25	−0.31
	N (3°)	−0.90	−0.69	−0.47	−0.56						
	N (2°)	−1.12	−0.81	−0.97	−1.04						
2e	P	2.73	1.61	1.36	1.51						
	O[b]	−1.10	−0.71	−0.67	−0.69						
	=O	−1.14	−0.63	−0.67	−0.83						
	N^+ (3°)	−0.86	−0.73	−0.42	−0.44						
	N (2°)	−1.16	−0.82	−0.82	−0.86						

[a] The carbon charges include the atomic charges of attached hydrogens. [b] Oxygen atom of the hydroxyl group.

Some of the intuitively reasonable arguments that can be made to rationalize PM reactivity as a function of pH are not borne out in the NPA charges. For example, our previous experimental results suggested that anionic PM (**3d**) protonates at the $N^{(1)}$ position to yield the zwitterionic form (**3e**). This protonation is coincident with slower cyclization to the aziridinium.[3] The NPA charge data does not provide an explanation for this reduction in activity since the nitrogen charges are predicted to be essentially constant for the different charge and protonation states (Tables 6). This suggests that the nucleophilicity of the nitrogen is not affected by protonation at other sites in the molecule. However, it should be emphasized that the predicted atomic charges in no way reflect the polarizability of the electron density, which can reasonably be expected to be much greater in the anionic than the zwitterionic states. Hence, the anionic PM species (**3d**) might be better able to "recruit" electrons from the phosphoramide moiety to stabilize the quaternary nitrogen

formed in the transition state to the aziridinium. This effect could be determined by calculating the charge densities at various points along the reaction path to aziridinium formation, but such calculations are beyond the scope of the present study.

The theoretical data, however, may provide a clue to another possible origin of the differential cyclization rates. The theoretical data suggests the electrophilicity of the β-carbons, rather than the nucleophilicity of the nitrogens, is modified by the protonation of the heteroatoms. Both the anionic IPM (**1c**) and PM (**3d**) species are predicted to have significantly longer C−Cl bonds (~1.82 Å) than the corresponding zwitterionic species **1d**, **3e** (~1.79 Å; Table 4). Differences between the anionic and neutral species are evident in the charges for the β-carbons and chlorines. For the neutral (**3a**) and zwitterionic PM (**3e**), the NPA charges for the β-carbons are ~+0.1, and for the chlorines, ~−0.1 (Table 6). In the anionic PM (**3d**), this charge separation has nearly doubled to +0.16 and −0.21 for the carbon and chlorine, respectively. This larger positive charge on the β-carbon should render it more electrophilic, while the increased negative charge on the chloride should make it a better leaving group (in a polar solvent).

Conclusions

The ^{31}P, ^{15}N, and ^{17}O NMR data suggest N-protonation of IPM with a pK_a of 4.3. These results are consistent with protonation of either the anionic IPM (**1c**) or the neutral species (**1a**) to yield the zwitterionic IPM (**1d**) or the cationic IPM (**1b**), respectively. The similarity in structure of IPM to phosphorodiamidic acid ($(H_2N)_2PO(OH)$), which is thought to exist as a zwitterion after N-protonation below its pK_a of 4.9[3,26] may argue in support of IPM protonation resulting in zwitterionic structure **1d**. This conclusion is also consistent with our previous studies on phosphoramide mustard.[3]

The determination of a pK_a of 5.3 for the IPM−aziridine supports the hypothesis that the lower alkylating activity of IPM is due, in part, to the formation of an aziridine ring at physiological pH and this species is relatively stable compared to an aziridinium ion. The different rates measured for the cyclization of PM when compared to IPM must be due to other factors which may include the polarizability of the C−Cl bond.

The finding that our theoretical models for the structure and thermodynamic stability of protonated phosphoramides,[3] PM, IPM, and IPM−aziridine correctly predict the experimental results certainly lend support for the continued use of these algorithms.

Experimental Section

Synthesis of Labeled Isophosphoramide Mustard. [$^{15}N_2$]Isophosphoramide mustard and [^{17}O]isophosphoramide mustard were prepared by published procedures.[4,5]

Aziridine was prepared in a 5 mm NMR tube from chloroethylamine by a modification of the procedure of Wystrach et al.[27] Briefly, 138 mg of 2-chloroethylamine hydrochloride (Aldrich Chemical Co.) in 0.28 mL of D_2O was mixed with 0.25 mL of 8.5 M NaOD and warmed to 47 °C. Two phases formed in the tube with the lower phase containing higher levels of aziridine as determined by ^1H NMR spectroscopy.

NMR Spectroscopy. NMR spectroscopy was performed on a Bruker MSL500 at 11.75 T. ^{31}P NMR spectroscopy at 202.5 MHz was performed with inverse-gated proton-decoupling over the acquisition time of 0.4 s with a sweep-width of 10 000 Hz and a relaxation delay of 1.6 s. ^{15}N NMR spectra at 50.7 MHz were acquired with inverse-gated proton decoupling or without decoupling and with a 20 000 Hz sweep width, a 25 ms acquisition time, and 0.2 s repetition time. Samples for ^{15}N and ^{31}P NMR spectroscopy were placed within 10 mm NMR tubes equipped with a coaxial insert containing 0.05 M [^{15}N]urea in 0.1 M sodium phosphate pH 7.0. ^{31}P spectra were referenced to this external phosphate resonance set to 0 ppm. ^{15}N spectra were referenced to the external [^{15}N]urea resonance set to 56.5 ppm (relative to the natural abundance ^{15}N resonance of 0.1 M ammonium hydroxide in 0.1 M sodium phosphate, pH 7.0 at 0 ppm). The ^{17}O NMR spectra were referenced to the internal natural abundance ^{17}O water resonance set to 0 ppm. The position of this resonance does not change with pH over the range studied.

Samples for NMR spectroscopy were dissolved in 0.1 M NaCl with 10% D_2O to a concentration between 10 and 30 mM. The solutions were immediately cooled in an ice-water bath. The pH meter was calibrated at 20 °C; however, all sample readings were performed in the ice−water bath. The pH was adjusted by the addition of 0.1 or 0.5 M solutions of NaOH or HCl. The pH of the samples were taken before and after the NMR experiment and agreed to within 0.1 pH unit. The pH values used are the average of the two readings and are not corrected for the deuterium concentration or temperature. The temperature was maintained at 4 ± 1 °C using the Bruker variable-temperature control unit.

One-bond $^{15}N-^1H$ coupling constants are negative; one-bond $^{15}N-^{31}P$ coupling constants can be positive or negative. All coupling constant data are measured directly from the NMR spectrum and are presented as absolute values.

Data Analysis. Titration data were fit to a monobasic titration curve using the nonlinear regression curve-fitting software in SigmaPlot (Jandel Scientific). The standard errors resulting from curve fitting are calculated by the program (see Figure 3 legend) and may underestimate the actual errors.[28] The pK_as and errors given in the Abstract, Discussion, and Conclusion sections are the average pK_a ± 1 standard deviation for at least three curve fits to separate sets of data.

Theoretical Calculations. The initial geometric structures were generated using a standard molecular mechanics program. All subsequent geometry optimization and electronic structure calculations were performed using the quantum chemistry program Gaussian 92.[29] The structures of all phosphoramide mustards and their various protonation states are shown in Figure 4. These structures were optimized at the Hartree−Fock (HF) level of theory using a 6−31G* basis set. Harmonic vibrational frequencies were calculated at these optimized geometries with the 6-31G* basis set to verify that the structures were true minima. Additionally, single-point energies were calculated at the optimized geometries using second-order Møller−Plesset perturbation theory (MP2) with a 6-31G** basis set. Mulliken populations, atomic charges fit to the electrostatic potential at the solvent-accessible surface, and solvation energies (*vide infra*) were also calculated with this larger basis set. Finally, NPA analysis was performed at the HF/6-31G** level of theory to provide atomic charges less sensitive to configuration and basis set effects.[21]

In order to model solvation effects, we have used a theoretical method based on the polarizable continuum model for solvents. This method was developed independently by Miertus and Tomasi[30] and Rashin.[31] Our implementation method is described in detail elsewhere.[32] The surrounding medium is treated as a continuum dielectric in a procedure involving several steps. First, the molecular geometry and electronic wave function are obtained from the Hartree−Fock calculation. Next, the interface between the molecule and the dielectric continuum of the surrounding medium is defined by the contact surface of the solvent molecule rolling around the scaled va der Waal's surface of the molecule. The boundary-element method is used to represent the triangulated surface, as developed by Zauhar and Morgan.[33] The electric potential is used to determine effective atomic charges (using a least-squares fit with constraints for net charge and dipole moments). Applying Gauss' law, the resulting electric field at the molecule surface (obtained from the atomic charges) is used

to determine the effective charge of the dielectric continuum at the surface. These induced charges at the surface are then included in the one-electron portion of the HF Hamiltonian and the wavefunction is reoptimized. New atomic charges are calculated from the reoptimized wave function, and the whole procedure is iterated to convergence (typically eight iterations). The surface charge is then used to determine the free energy of hydration. The surface area and volume of the molecule is used in an approximate expression to determine the free energy of cavitation (the nonelectrostatic energy to create a cavity in the dielectric continuum containing the molecule). The theoretical free energy of solvation is calculated by summing the free energy of hydration and the free energy of cavitation.

Studies of the performance of this model[32,34] indicates that it predicts absolute ΔG_{solv}'s accurate to 5 kcal/mol for several neutral, ionic, and zwitterionic compounds. Larger errors of up to 11 kcal/mol occur for small nonpolar molecules such as neutral trimethylamine where ΔG_{solv} is not dominated by electrostatic solute–solvent interactions. For these compounds, dispersion and solvent reorganization energies, not included in these predictions, act to cancel out the cavitation energy.

Acknowledgment. This work was supported by Public Health Service Grants CA51229 (M.P.G.), CA16783 (O.M.C.), and CA09243-14 (training grant to E.M.S.-R.) from the National Cancer Institute, Department of Health and Human Services, and the American Cancer Society Institutional Research Grant No. IRG-32 (S.M.L.). This work was carried out in part at the Sandia National Laboratory (M.E.C.) under contract from the U.S. Department of Energy and supported by its Division of Basic Energy Sciences.

Supplementary Material Available: The ^{31}P and ^{15}N chemical shift versus pH titration curves for IPM and IPM–aziridine, the ^{17}O chemical shift versus pH titration curve for IPM, and the complete Z-matrices for the Hartree–Fock 6-31G* optimized structures as well as the complete table of atomic charges for the structures shown in Figure 4 (15 pages). Ordering information is given on any current masthead page.

References

(1) Boal, J. H.; Williamson, M.; Boyd, V. L.; Ludeman, S. M.; Egan, W. ^{31}P NMR Studies of the Kinetics of Bisalkylation by Isophosphoramide Mustard: Comparisons with Phosphoramide Mustard. *J. Med. Chem.* **1989**, *32*, 1768–1773.

(2) Colvin, M.; Chabner, B. A. In *Cancer Chemotherapy: Principles and Practice*; Chabner, B. A., Collins, J. M., Eds.; J. B. Lippincott Co.: Philadelphia, 1990; pp 276–313.

(3) Gamcsik, M. P.; Ludeman, S. M.; Shulman-Roskes, E. M.; McLennan, I. J.; Colvin, M. E.; Colvin, O. M. Protonation of Phosphoramide Mustard and Other Phosphoramides. *J. Med. Chem.* **1993**, *36*, 3636–3645.

(4) Shulman-Roskes, E. M.; Gamcsik, M. P.; Colvin, O. M.; Chang, Y. H.; Koo, K. I.; Ludeman, S. M. Synthesis of ^{15}N Labelled Isophosphoramide Mustard. *J. Labelled Compd. Radiopharm.* **1994**, *34*, 231–237.

(5) Han, S. Y.; Shulman-Roskes, E. M.; Misiura, K.; Anderson, L. W.; Szymajda, E.; Gamcsik, M. P.; Chang, Y. H.; Ludeman, S. M. Synthesis of ^{17}O (and ^{18}O) Labelled Isophosphoramide Mustard. *J. Labelled Compd. Radiopharm.* **1994**, *34*, 247–254.

(6) Zheng, J. J.; Chan, K. K.; Muggia, F. Preclinical Pharmacokinetics and Stability of Isophosphoramide Mustard. *Cancer Chemother. Pharmacol.* **1994**, *33*, 391–398.

(7) Watson, E.; Dea, P.; Chan, K. K. Kinetics of Phosphoramide Mustard Hydrolysis in Aqueous Solution. *J. Pharm. Sci.* **1985**, *74*, 1283–1292.

(8) Golding, B. T.; Kebbell, M. J.; Lockhart, I. M. Chemistry of Nitrogen Mustard [2-Chloro-N-(2-chloroethyl)-N-methylethanamine] Studied by Nuclear Magnetic Resonance Spectroscopy. *J. Chem. Soc., Perkin Trans 2* **1987**, 705–713.

(9) Gamcsik, M. P.; Hamill, T. G.; Colvin, M. NMR Studies of the Conjugation of Mechlorethamine with Glutathione. *J. Med. Chem.* **1990**, *33*, 1009–1014.

(10) Engle, T. W.; Zon, G.; Egan, W. ^{31}P NMR Kinetic Studies of the Intra- and Intermolecular Alkylation Chemistry of Phosphoramide Mustard and Cognate N-Phosphorylated Derivatives of N,N-Bis(2-chloroethyl)amine. *J. Med. Chem.* **1982**, *25*, 1347–1357.

(11) Reed, A. E.; Schleyer, P. v. R. Chemical Bonding in Hypervalent Molecules. The Dominance of Ionic Bonding and Negative Hyperconjugation over d-Orbital Participation. *J. Am. Chem. Soc.* **1990**, *112*, 1434–1445.

(12) Karle, I. L.; Karle, J. M.; Egan, W.; Zon, G.; Brandt, J. A. Absolute Configuration of (+)-Cyclophosphamide. A Crystal and Molecular Structure Determination by X-ray Diffraction. *J. Am. Chem. Soc.* **1977**, *99*, 4803–4807.

(13) Garcia-Blanco, S.; Perales, A. The Crystal Structure of N,N-Bis-2-chloroethyl-N'-propylene Phosphoric Ester Diamide Monohydrate (Endoxan). *Acta Crystallogr.* **1972**, *B28*, 2647–2652.

(14) Camerman, A.; Smith, H. W.; Camerman, N. Activated Cyclophosphamide Anticancer Drugs: Molecular Structures of cis- and trans-4-Hydroperoxyisophosphamides. *J. Med. Chem.* **1983**, *26*, 679–683.

(15) Szabo, A.; Ostlund, N. S. *Modern Quantum Chemistry: Introduction to Modern Electronic Structure Theory*; Macmillan: New York, 1989; p 200.

(16) Locke, M. J.; Hunter, R. L.; McIver, R. T., Jr. Experimental Determination of the Acidity and Basicity of Glycine in the Gas Phase. *J. Am. Chem. Soc.* **1979**, *101*, 272–273.

(17) Locke, M. J.; McIver, R. T., Jr. Effect of Solvation on the Acid/Base Properties of Glycine. *J. Am. Chem. Soc.* **1983**, *105*, 4226–4232.

(18) Friedman, O. M.; Myles, A.; Colvin, M. Cyclophosphamide and Related Phosphoramide Mustards. Current Status and Future Prospects. *Adv. Cancer Chemother.* **1979**, *1*, 143–204.

(19) Friedman, O. M. Studies of Some Newer Phosphoramide Mustards. *Cancer Chemother. Rep.* **1967**, *51*, 347–357.

(20) *Population Analysis and Electron Densities from Quantum Mechanics*; Lipkowitz, K. B., Boyd, D. B., Eds.; VCH Publishers, Inc.: New York, 1994; Vol. V.

(21) Reed, A. E.; Weinstock, R. B.; Weinhold, F. Natural Population Analysis. *J. Chem. Phys.* **1985**, *83*, 735–746.

(22) Cox, S. R.; Williams, D. E. Representation of the Molecular Electrostatic Potential by a Net Atomic Charge Model. *J. Comput. Chem.* **1981**, *2*, 304–323.

(23) Singh, U. C.; Kollman, P. An Approach to Computing Electrostatic Charges of Molecules. *J. Comput. Chem.* **1984**, *5*, 129.

(24) Cohen, B.; van Artsdalen, E. R.; Harris, J. Reaction Kinetics of Aliphatic Tertiary β-Chlorethylamines in Dilute Aqueous Solution. I. The Cyclization Process. *J. Am. Chem. Soc.* **1948**, *70*, 281–285.

(25) Zon, G.; Ludeman, S. M.; Egan, W. High Resolution Nuclear Magnetic Resonance Investigations of the Chemical Stability of Cyclophosphamide and Related Phosphoramidic Compounds. *J. Am. Chem. Soc.* **1977**, *99*, 5785–5795.

(26) Rahil, J.; Haake, P. Reactivity and Mechanism of Hydrolysis of Phosphonamides. *J. Am. Chem. Soc.* **1981**, *103*, 1723–1734.

(27) Wystrach, V. P.; Kaiser, D. W.; Schaefer, F. C. Preparation of Ethylenimine and Triethylenemelamine. *J. Am. Chem. Soc.* **1955**, *77*, 5915–5918.

(28) Motulsky, H. J.; Ransnas, L. A. Fitting Curves to Data Using Nonlinear Regression: A Practical and Nonmathematical Review. *FASEB J.* **1987**, *1*, 365–374.

(29) Frisch, M. J.; Trucks, G. W.; Head-Gordon, M.; Gill, P. M. W.; Wong, M. W.; Foresman, J. B.; Johnson, B. G.; Schlegel, H. B.; Robb, M. A.; Repogle, E. S.; Gomperts, J. L.; Adres, J. L.; Raghavachari, K.; Binkley, J. S.; Gonzalez, C.; Martin, R. L.; Fox, D. J.; Defrees, D. J.; Baker, J.; Stewart, J. J. P.; Pople, J. A. In Gaussian, Inc.: Pittsburgh, 1992.

(30) Miertus, S.; Scrocco, E.; Tomasi, J. Electrostatic Interaction of a Solute with a Continuum. A Direct Utilization of Ab Initio Molecular Potentials for the Prevision of Solvent Effects. *Chem. Phys.* **1981**, *55*, 117–129.

(31) Rashin, A. A.; Namboodiri, K. A. Simple Method for the Calculation of Hydration Enthalpies of Polar Molecules with Arbitrary Shapes. *J. Phys. Chem.* **1987**, *91*, 6003–6012.

(32) Colvin, M. E.; Melius, C. E. Continuum Solvent Models for Computational Chemistry. *Sandia National Laboratories* **1993**, *SAND93-8239*, 1–34.

(33) Zauhar, R. J.; Morgan, R. S. Computing the Electric Potential of Biomolecules: Application of a New Method of Molecular Surface Triangulation. *J. Comput. Chem.* **1990**, *11*, 602–622.

(34) Evleth, E. M.; Akacem, Y.; Colvin, M. Comparison of ab initio and AMSOL Semiempirical Free Energies of Solvation for Third-row Species. *Chem. Phys. Lett.* **1994**, *227*, 412–418.

(35) Gadian, D. G.; Radda, G. K.; Richards, R. E.; Seeley, P. J. In *Biological Applications of Manetic Resonance*; Shulman, R. G., Ed.; Academic Press, Inc.: New York, 1979; pp 463–535.

(36) Duthaler, R. O.; Roberts, J. D. Steric and Electronic Effects on the ^{15}N Chemical Shifts of Saturated Aliphatic Amines and Their Hydrochlorides. *J. Am. Chem. Soc.* **1978**, *100*, 3889–3895.

(37) Gerothanassis, I. P.; Sheppard, N. Natural-Abundance ^{17}O NMR Spectra of Some Inorganic and Biologically Important Phosphates. *J. Magn. Reson.* **1982**, *46*, 423–439.

JM940839N